

E18-2007-110

Yu. V. Taran, A. M. Balagurov, A. N. Kuznetsov,
J. Schreiber¹, H. Bomas², Ch. Stoeberl², P. Rathjen²,
W. J. J. Vorster³, A. M. Korsunsky³

INVESTIGATION OF IN-PLANE BIAXIAL LOW CYCLE
FATIGUED AUSTENITIC STAINLESS STEEL AISI 321.
I. MECHANICAL TESTING ON THE PLANAR BIAXIAL
LOAD MACHINE

¹Fraunhofer Institute for Non-Destructive Testing, Dresden branch, Germany

²Division of Material Science, Foundation Institute for Materials Science,
Bremen, Germany

³Department of Engineering Science, University of Oxford, UK

Таран Ю. В. и др.

E18-2007-110

Исследование аустенитной нержавеющей стали AISI 321, подвергнутой плоскостному двухосному низкочастотному усталостному циклированию. I. Механические испытания на планарной двухосной нагрузочной машине

Под действием усталостной нагрузки в материалах происходят изменения в микроструктуре, которые влияют на их механические и физические свойства. Экспериментальное моделирование изменений может выполняться циклической механической нагрузкой, обычно в форме одноосного растяжения-сжатия. Однако реальные машины и структуры подвергаются более сложным многоосным напряжениям. Исследования усталостных свойств материалов и их разрушение под действием многоосных нагрузок являются одной из актуальных тем, нацеленных на повышение надежности промышленных компонентов. Первым шагом к лучшему пониманию этой проблемы является тестирование материалов под действием двухосной нагрузки. Набор крестообразных образцов из нержавеющей аустенитной стали AISI 321 был подвергнут циклическому растяжению-сжатию с частотой 0,5 Гц при нагрузке 10–17 кН. Образцы были предназначены для исследований методом нейтронной дифракции.

Работа выполнена в Лаборатории нейтронной физики им. И. М. Франка ОИЯИ.

Сообщение Объединенного института ядерных исследований. Дубна, 2007

Taran Yu. V. et al.

E18-2007-110

Investigation of In-Plane Biaxial Low Cycle Fatigued Austenitic Stainless Steel AISI 321. I. Mechanical Testing on the Planar Biaxial Load Machine

During fatigue loading of structural materials such as stainless steel, changes in the microstructure which affect the mechanical and physical properties occur. Experimental simulation of the loading conditions that induce the changes can be performed by mechanical loading, usually in the form of uniaxial tension–compression cycling. However, real machines and structures are subjected to more complex multiaxial stresses. Fatigue and fracture under multiaxial stresses are one of the most important current topics aimed at ensuring improved reliability of industrial components. The first step towards better understanding of this problem is to subject the materials to biaxial loading. The material examined was low austenitic stainless steel AISI 321 H. A set of the four samples of cruciform geometry was subjected to the biaxial tension–compression fatigue cycling with the frequency of 0.5 Hz at the applied load of 10–17 kN. The samples are intended for the neutron diffraction measurements of the residual stresses and the mechanical characterizations on a dedicated stress-diffractometer.

The investigation has been performed at the Frank Laboratory of Neutron Physics, JINR.

Communication of the Joint Institute for Nuclear Research. Dubna, 2007

CONTENTS

Introduction	1
1. Material and Samples	2
2. Mechanical Testing	4
2.1. Sample Kreuz-1	7
2.1.1. Uniaxial Quasistatic Tensile Testing	7
2.1.2. In-Plane Biaxial Quasistatic Tension–Compression Testing	8
2.1.3. In-Plane Biaxial LCF Tension–Compression Testing	8
2.1.4. Residual Macrostrain during the Step-by-Step Biaxial Cycling	13
2.2. Sample Kreuz-2	13
2.2.1. In-Plane Biaxial LCF Tension–Compression Testing	13
2.2.2. Residual Macrostrain during the Step-by-Step Biaxial Cycling	15
2.3. Sample Krest-1	16
2.3.1. In-Plane Biaxial LCF Tension–Compression Testing	16
2.4. Sample Krest-2	16
2.4.1. In-Plane Biaxial LCF Tension–Compression Testing	18
Conclusion	20
References	24

INTRODUCTION

During fatigue loading of constructional materials changes in the microstructure which affect the mechanical and physical properties occur. The experimental simulation of these changes can be performed by cyclic mechanical loading, usually by uniaxial tension–compression fatigue cycling. However, machines and structures are usually subjected to complex multiaxial stresses rather than to simple uniaxial stress. Multiaxial stress occurs either due to multiaxial loading or to a locally induced multiaxial stress state. The failure and fracture problem under multiaxial stresses is one of the most important topics to ensure the reliability of industrial components. The first step in the deciphering of this problem is to subject the materials to biaxial loading, e.g., to in-plane biaxial or coaxial tension–torsion fatigue. It is necessary to note the inability of conventional uniaxial load simulation plus classical yield criteria to adequately predict in-service fatigue failures [1]. Design engineers are in need of assisting tools to evaluate the constraint of the materials under multiaxial loading conditions. The area of simulation of multiaxial stress fields covers a very wide range of experimental techniques which are focused on investigating the behaviour of materials with various specimen geometries.

Construction materials, research of which is important, are first of all a stainless steel, a duplex-phase steel, a shape-memory alloy, etc. A low carbon Ti-stabilized chrome–nickel austenitic stainless steel (ASS) of AISI 321 type is of special interest due to the outstanding properties, in particular, high corrosion resistance, mechanical and welding characteristics. The steel is widely used in highly technological and potentially dangerous industries, for example, in nuclear industry and nuclear power generation plants. However, a major problem in a number of applications is multiaxial loading fatigue degradation and martensitic transformation of ASS components. The assessment of the actual fatigue damage and, thus, the remaining fatigue lifetime of material is a task of great practical relevance.

Many investigations using the conventional and radiation (X-ray- and neutron diffraction (ND)) methods show the influence of material history (founding, annealing, quenching, etc.) and fatigue cycling conditions (load amplitude, frequency, stress or strain control, temperature, value of R-ratio, number of cycles, etc.) on the fatigue properties of ASS. The ND method is a powerful tool for investigations of fatigue properties of multiphase industrial materials due to its phase sensitivity. Before, the ND research of the steel AISI 321 subjected to uniaxial low and high cycle fatigue (LCF/HCF) was carried out on the ENGIN and ENGIN-X stress-diffractometers at the ISIS neutron pulsed facility in the frame of the collaboration of JINR and FINT [2–9]. The idea of the ND method application for research of materials subjected to biaxial load fatigue cycling was for the first time discussed on the Stainless Steel World 2005 Conference [8],

and then a little in more detail on the 7th European Conference on Residual Stresses [9]. The aims of proposed strain scanning and *in-situ* stress rig experiments are a study of the fatigue degradation and the martensite transformation of the steel AISI 321 during the in-plane biaxial LCF, especially the residual stresses 2D mapping, the mechanical testing of austenite and martensite phases in elastic and plastic regions. For that, several samples of a cruciform geometry were *ex-situ* subjected to biaxial load cycling at a frequency of 0.5 Hz at FIMS.

The present work is the 1st part of the paper «Investigation of In-Plane Biaxial Low Cycle Fatigued Austenitic Stainless Steel AISI 321» that describes a mechanical testing of the cruciform samples at FIMS (Bremen) in September 2006. The 2nd part of the paper will describe the neutron diffraction stress analysis of one of the *ex-situ* fatigued cruciform samples performed at the IBR-2 nuclear pulsed reactor (FLNP JINR) in November–December 2006.

1. MATERIAL AND SAMPLES

The material examined in this work was a low carbon Ti-alloyed metastable austenitic stainless steel of the Russian grade GOST 12X18H10T (which is an analogue of the US grade AISI 321 H). The steel was delivered as a hot-rolled sheet with a thickness of 16 mm. The chemical composition is presented in

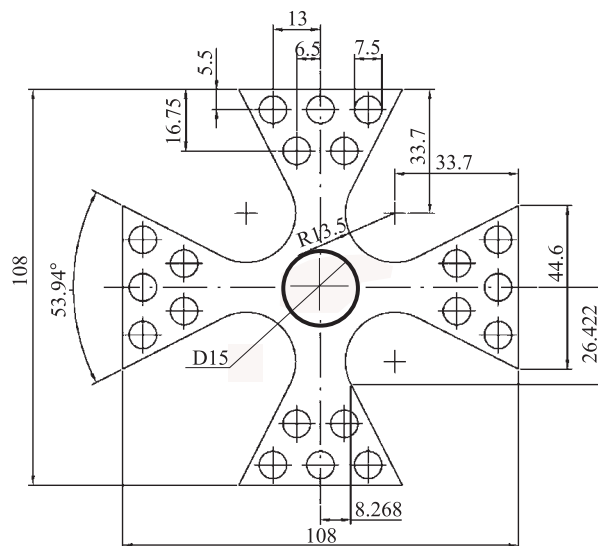


Fig. 1. Sample of the cruciform geometry (Kreuz) designed at FIMS; thickness of a sample and a membrane of the 15 mm diameter were 5 and 2 mm, respectively

Table 1. Chemical composition of the steel 12X18H10T

Elements	C	Mn	Si	S	P	Cr	Ni	Ti	Mo	V	W
Weight, %	0.07	0.65	0.40	0.009	0.039	17.78	9.41	0.42	0.09	0.05	0.03

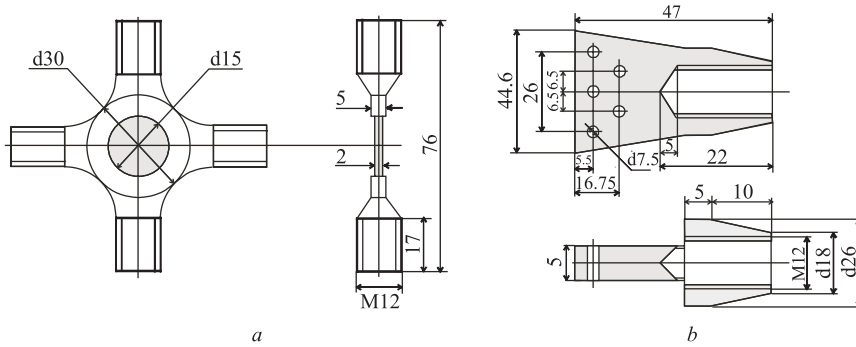


Fig. 2. Sample of the cruciform geometry (Krest) designed at FLNP (a) and a clamp (b) to fix Krest in a biaxial testing machine

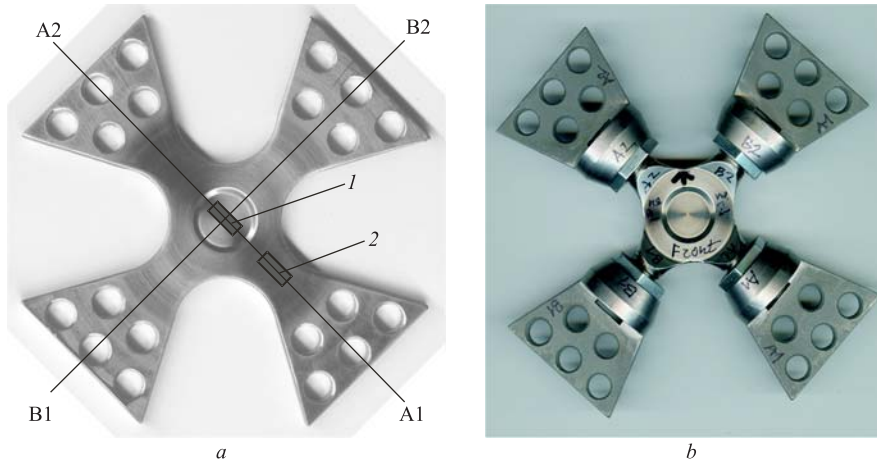


Fig. 3. a) Sample Kreuz-1 of the FIMS design. The front side: 1 — A_{front} gage on the membrane, 2 — A_{leg} gage on the leg; b) sample Krest-1 of the cruciform geometry of the FLNP design

Table 1. The yield stress $R_{p0.2}$ and the tensile strength R_m were defined by the producer to be equal to 370 and 580 MPa, respectively.

A design of a sample of the cruciform geometry was made at FIMS (Fig. 1). Hereinafter we shall name the sample of the FIMS design as the Kreuz. Using the design and testing experience of FIMS a new sample of the cruciform geometry was designed at FLNP (Fig. 2). We shall name the sample of the FLNP design as the Krest.

The two pairs of the samples were machined in the FLNP workshop under the FIMS and FLNP designs, respectively (Fig. 3 (*a, b*)).

2. MECHANICAL TESTING

Testing Machine. The mechanical testing of all samples was performed on the Instron 100 kN biaxial planar cruciform system at FIMS (Fig. 4). The system belongs to the group of servohydraulic fatigue testing machines. The characteristics of the machine are the two load axes, which are composed of four separately controllable hydraulic actuators. Two opposite located actuators build one load-axis. The two axes are arranged in perpendicular direction and the sample is fixed in the intersection point of the axes as shown in Fig. 4. The actuators have a stroke of 20 mm, so the samples can be mounted and removed easily. Each actuator has one load cell with acceleration force compensation. The load cells are designed for a static load of 100 kN and in case of dynamic tests — for a maximal load of 80 kN. Thereby, the frequency can be changed continuously up to 50 Hz. The loads can be applied on the sample in-phase or out-of-phase. The shape of the load cycle can be varied between sine, triangle

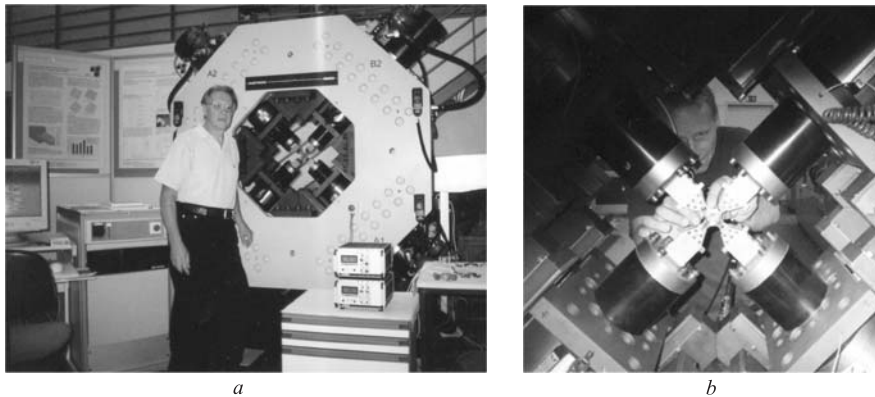


Fig. 4. Instron 100 kN biaxial planar cruciform system at FIMS: *a* — front view; *b* — actuators and supports of a sample

function or rectangle function. During the cycling the axes are linked together by modal control. Therefore, the translation of the sample in the centre of the machine is minimized. For example, at a load of 80 kN and a frequency of 50 Hz the translation of the sample centre is smaller than 2%. Two servo-valve kits with a flux rate of 40 l/min for high deformation and 10 l/min for low deformation are available. The shape of the sample is like a cross. Depending on the configuration of the clamps, the samples size can be varied between 100×100 mm and 300×300 mm. The thickness of the tested sample is arbitrary. The centre of the sample builds the tested volume and can be designed differently. The state of stress in the centre of the sample depends on its shape and has to be calculated by the finite element method.

Strain Gages. To control the applied load–macrostrain responses of a tested sample two types of a strain gage were used. The FLA-5-11 strain gage is designed for steel substrates. The length of the strain gages was 5 mm. The resistances were 120 ± 0.3 Ohm. The strain gage factor was $2.11 \pm 1\%$. These gages were used to control the Kreuz-1 sample. In the centre of the Kreuz-2 sample, on each side of the membrane, the FCA-5-11 rosette stain gages were mounted. This type has two strain gages with a length of 5 mm lying perpendicular on top of each other. So, the strain of both load axes can be measured. The resistance was 120 ± 0.5 Ohm and the gage factor was $2.12 \pm 1\%$. The strain gages were fixed on the sample with a one-component cyanoacrylate adhesive named Sicomet®. During the measurement the strain gages on the sample were separately connected in quarter bridges. The carrier frequency of the testing bridge was 5 kHz, the input voltages were set to 5 V.

Tresca Criterion. A testing of a cruciform sample is possible in two modes: the in-phase (tension–tension) and out-of-phase (tension–compression) loads, respectively. The initial estimation of an applied stress ensuring an output in a plastic zone was obtained with the use of the Tresca criterion:

$$|\sigma_{\max} - \sigma_{\min}| \leq \sigma_Y,$$

where σ_{\max} and σ_{\min} are maximal and minimal values in a triaxial applied stress tensor, respectively, σ_Y is the yield stress ($R_{p0.2}$). In the case of a biaxial load, the tensor includes only two stress components σ_1 and σ_2 . The third component σ_3 is equal to 0. The results are the following: 1) the in-phase load: $\sigma_1 > 0$, $\sigma_2 > 0$, $\sigma_{\max} = \sigma_1 = \sigma_2$, $\sigma_{\min} = 0$, then $\sigma_1 \leq \sigma_Y$; 2) the out-of-phase load: $\sigma_1 > 0$, $\sigma_2 < 0$, $|\sigma_1| = |\sigma_2|$, $\sigma_{\max} = \sigma_1$, $\sigma_{\min} = -\sigma_1$, then $\sigma_1 \leq 1/2\sigma_Y$. Thus, the out-of-phase mode is more preferable from the point of view of minimization of the applied load.

The Von Mises criterion has given a closely related estimation for the 2nd mode:

$$\sigma_1 \leq 1/(3)^{1/2}\sigma_Y \approx 0.58\sigma_Y.$$

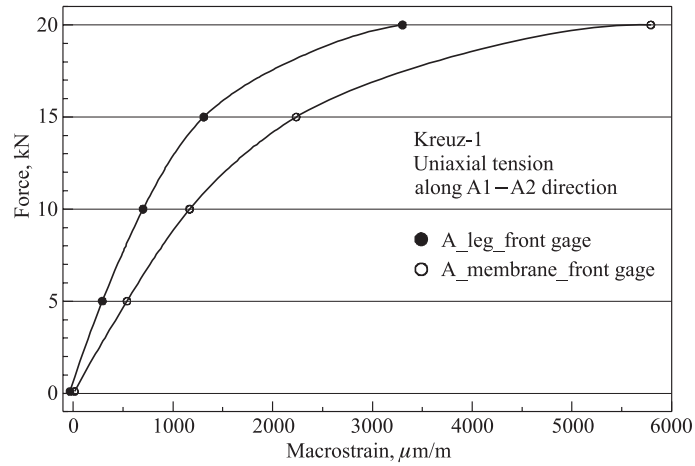


Fig. 5. Applied load–macrostrain responses of Kreuz-1 during the uniaxial tensile testing

Finite Element Analysis. The complicated configuration of a cruciform sample does not allow one to make a realistic estimation of a force necessary for achievement of a plastic zone. In this case, the elastic–plastic stress analysis by the finite element method (FEM) with using the ABACUS code was performed for the out-of-phase mode. The calculation has shown that the output in a plastic zone occurs at the force of 10–12 kN.

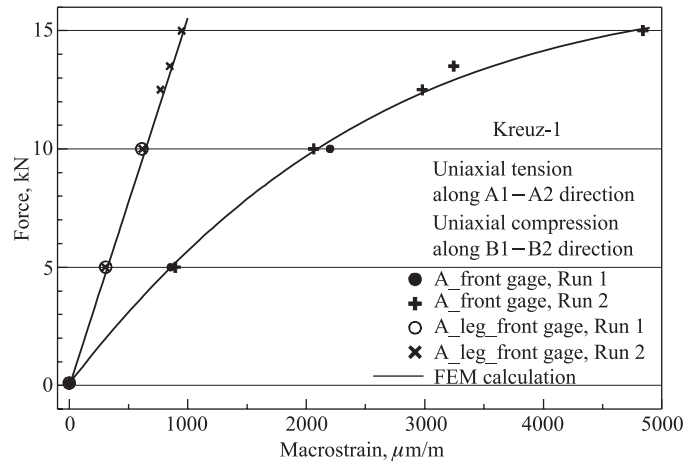


Fig. 6. Applied load–macrostrain responses of Kreuz-1 during the biaxial quasistatic tension–compression testing

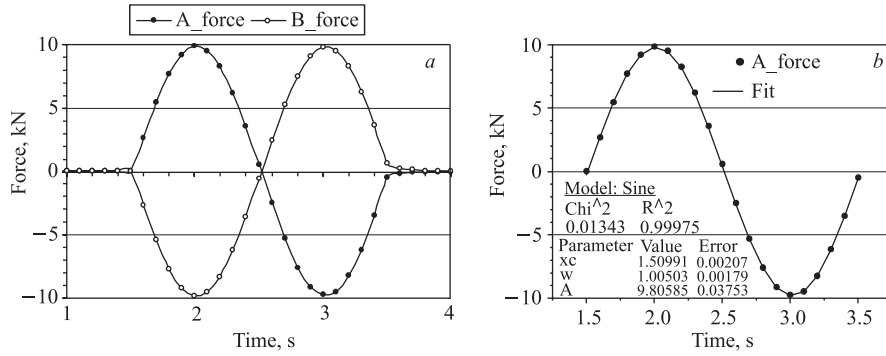


Fig. 7. *a*) Biaxial tension–compression loads applied to Kreuz-1 (1st step); *b*) modelling of the load applied to Kreuz-1 along the A1–A2 direction

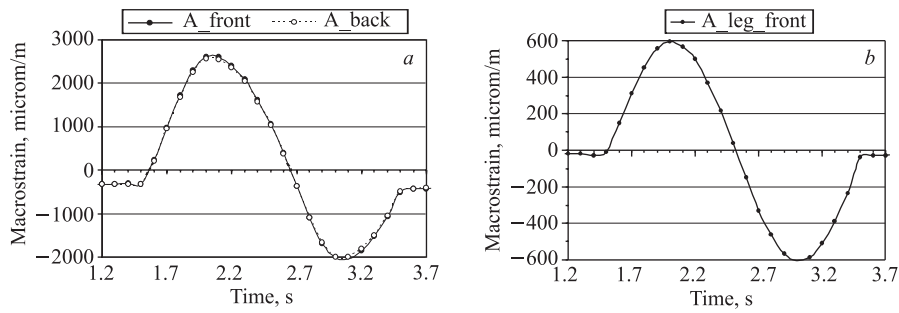


Fig. 8. Signals of the strain gages on Kreuz-1: *a* — the A_{front} and A_{back} gages on the membrane, respectively; *b* — the A_{leg_front} gage on the front side of the A1_{leg}

2.1. Sample Kreuz-1.

Placement of the Strain Gages. The three FLA-5-11 strain gages were placed on Kreuz-1 along the A1–A2 direction (Fig. 3, *a*): 1) the A_{front} gage on the front side of the membrane, 2) the A_{back} gage on the back side of the membrane, 3) the A_{leg_front} gage on the front side of the leg.

2.1.1. Uniaxial Quasistatic Tensile Testing. The two opposite legs of the sample were fixed in the Instron machine along the A1–A2 direction and the tensile load was applied along the same direction. The legs along the B1–B2 direction were not held in the machine. The applied load–macrostrain responses are shown in Fig. 5 for both front strain gages.

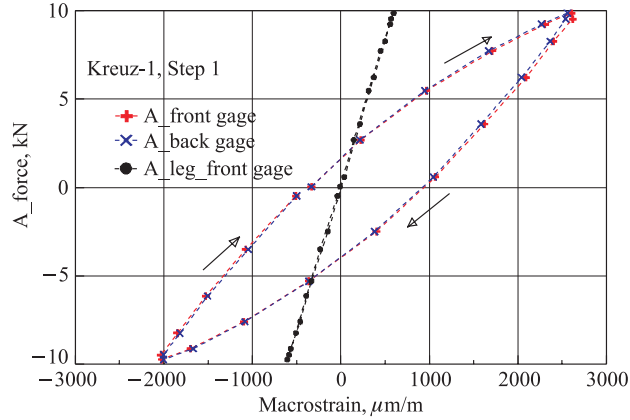


Fig. 9. Applied load-macrostrain responses of all strain gages on Kreuz-1 (1st step)

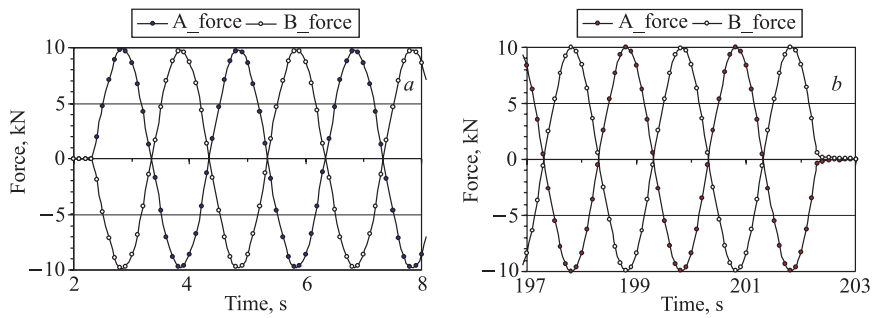


Fig. 10. Biaxial tension-compression load during the 2nd step: *a* — beginning; *b* — ending

2.1.2. In-Plane Biaxial Quasistatic Tension-Compression Testing.

Test of the Out-of-Phase Mode. After the uniaxial quasistatic tensile testing the legs along the B1-B2 direction were also fixed in the machine. The tensile load was applied along the A1-A2 direction and the compression load of the same absolute value was applied along the B1-B2 direction. The applied load-macrostrain responses are shown in Fig. 6 for both front strain gages.

FEM Modelling. The results of FEM modelling at $E = 170$ GPa, $\nu = 0.3$ and $\sigma_Y = 450$ MPa are shown in Fig. 6. The agreement with experimental data is excellent.

2.1.3. In-Plane Biaxial LCF Tension-Compression Testing.

After the analysis of results presented in Figs. 5 and 6 it was decided to begin the biaxial LCF testing at the load of 10 kN corresponding to the onset of plastic

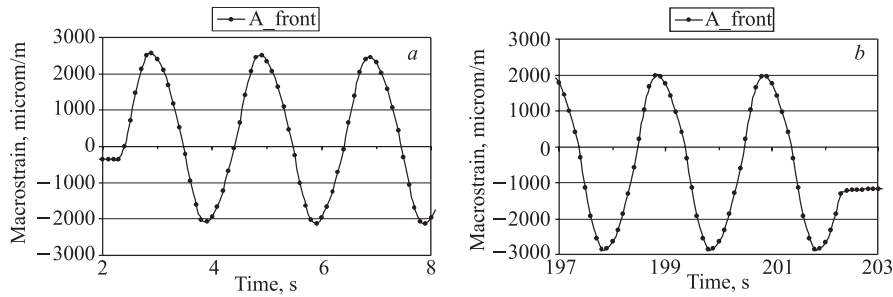


Fig. 11. Signal of the strain gage on the front side of the membrane: *a* — beginning of the 2nd step; *b* — ending of the 2nd step

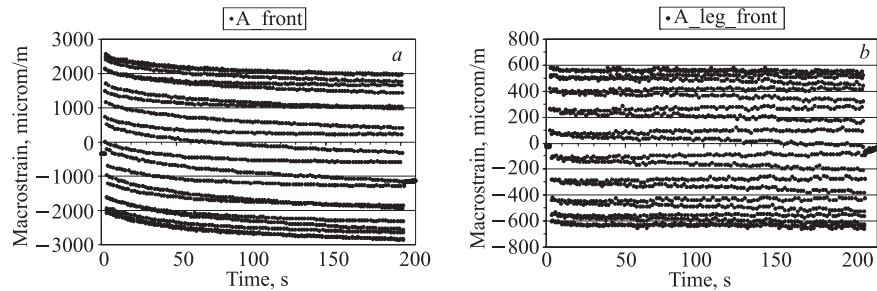


Fig. 12. Signals of the strain gages on the front side of Kreuz-1: *a* — A_front gage on the membrane; *b* — A_leg_front gage on the A1.leg (2nd step)

deformation (Fig.6). The cycling of the sample was made step by step at the frequency of 0.5 Hz.

- 1st step: the load of 10 kN, the step cycle number of 1.

During this step only one cycle was made to check a reaction of the load control devices of the machine (Fig.7, *a*) and the strain gages placed on the sample (Fig.8). The load along the A1–A2 direction is well described by the sine function (Fig.7, *b*). The applied load–macrostrain responses of all gages are shown in Fig.9.

- 2nd step: the load of 10 kN, the step cycle number of 100, the full cycle number of 101.

Indicated values of the load control devices and the strain gages during the 2nd step are shown in Figs.10–12. The applied load–macrostrain responses of the gages placed on the membrane are shown in Fig.13.

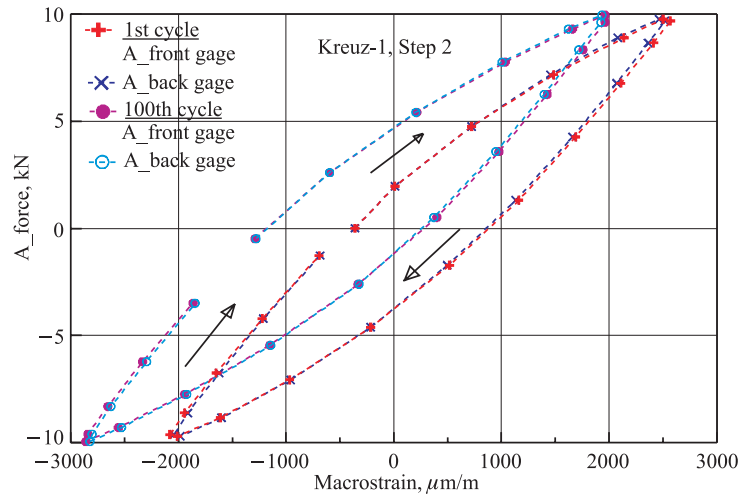


Fig. 13. Applied load–macrostrain responses of the strain gages on the membrane (2nd step)

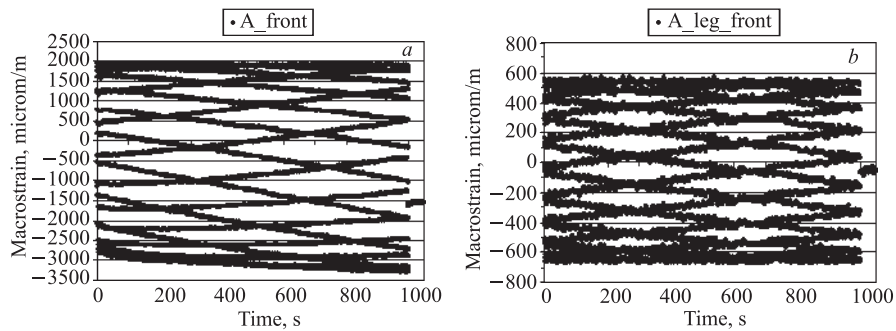


Fig. 14. Signal of the strain gage on the front side of Kreuz-1: *a* — A_{front} gage on the membrane; *b* — A_{leg_front} gage on the A1_{leg} (3rd step)

The reading frequency of the signals from the load control devices and the strain gages was equal to 10 Hz. In this case, the information on the amplitude of the signal could be received with sufficient accuracy. In Fig. 12, presenting the time dependences of the signals from the strain gages during the 2nd step, the higher and lower curves reflect the maximal and minimal values of the signal, respectively.

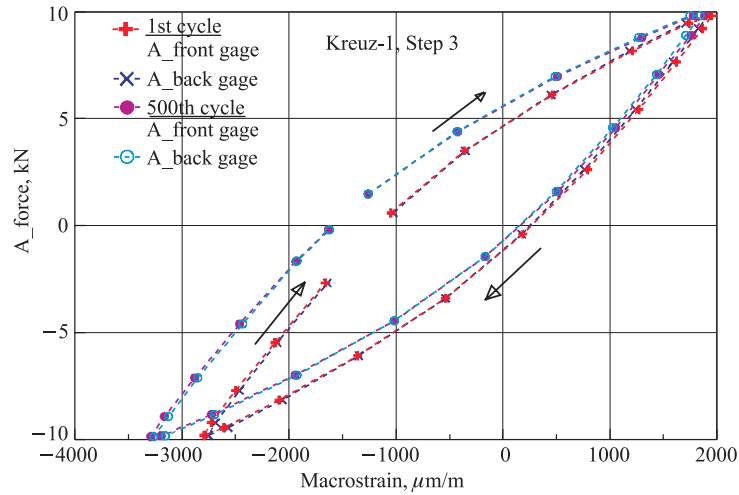


Fig. 15. Applied load–macrostrain responses of the strain gages on the membrane (3rd step)

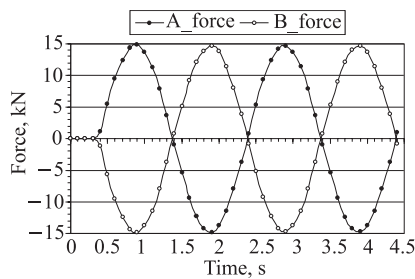


Fig. 16. Biaxial tension–compression loads applied to Kreuz-1 (4th step)

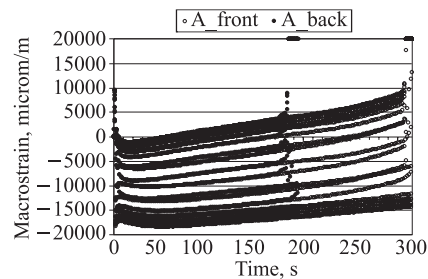


Fig. 17. Signals of the gages on the front and back sides of the membrane (4th step)

- 3rd step: the load of 10 kN, the step cycle number of 500, the full cycle number of 601.

Indicated values of the strain gages on the membrane and the leg during the 3rd step are shown in Fig. 14. The applied load–macrostrain responses of the gages placed on the membrane are shown in Fig. 15.

After ending of the 3rd step the martensite fraction was qualitatively estimated on the interaction force of a permanent magnet probe with the sample membrane. The force has appeared rather small contrary to expectations. The further cycling was continued with load amplitude increased up to 15 kN.

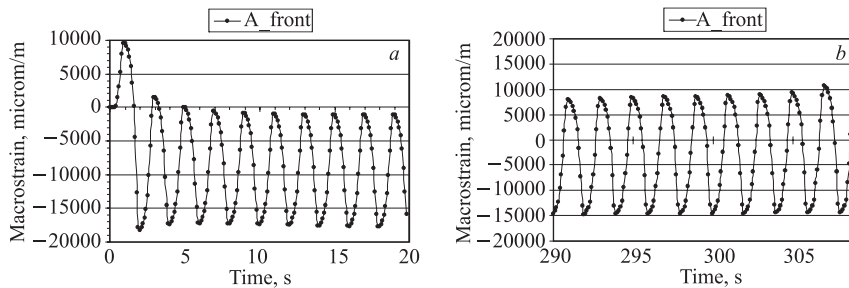


Fig. 18. Signal of the strain gage on the front side of the membrane: *a* — beginning of the 4th step; *b* — before the gage crash during the 4th step

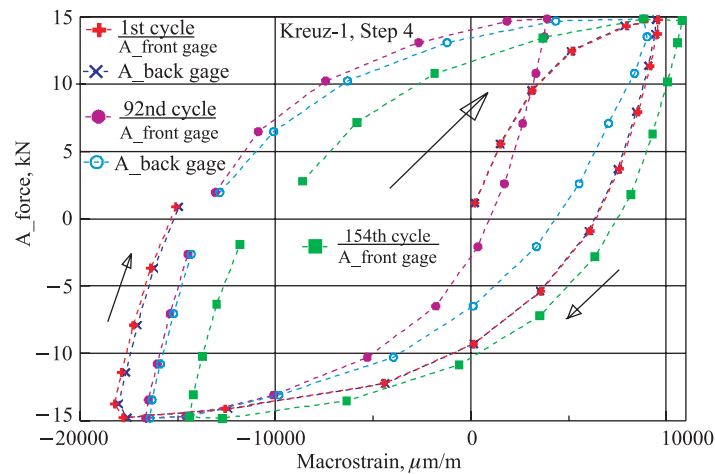


Fig. 19. Applied load–macrostrain responses of the strain gages on the membrane (4th step)

- 4th step: the load of 15 kN, the step cycle number of 500, the full cycle number of 1101.

In this step the loads were increased up to 15 kN. Indicated values of the load control devices and the strain gages during the 4th step are shown in Figs. 16–18.

Approximately on the 185 s (the 93rd cycle), the strain gage on the back side of the membrane has not stood the test (Fig. 17), and then the strain gage on the front side was also out of action (the 155th cycle, Figs. 17–18). The applied load–macrostrain responses of the gages placed on the membrane are shown in Fig. 19.

- 5th step: the load of 15 kN, the step cycle number of 500, the full cycle number of 1601.

As both strain gages on the membrane were out of action only the signal of the strain gage on the front side of the A1_leg is shown in Fig. 20.

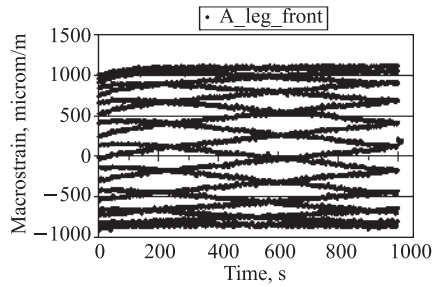


Fig. 20. Signal of the strain gage on the front side of the A1_leg (5th step)

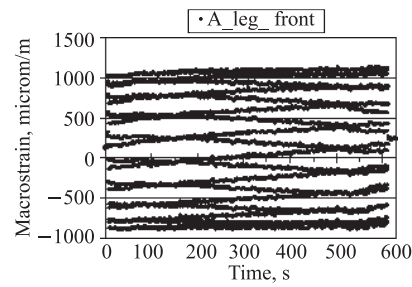


Fig. 21. Signal of the strain gage on the front side of the A1_leg (6th step)

- 6th step: the load of 15 kN, the step cycle number of 303, the full cycle number of 1904.

The signal of the strain gage on the front side of the A1_leg is shown in Fig. 21. On the 303rd cycle, the membrane has not stood the test and burst on a circle (Fig. 22). The cycling was stopped. Thus, Kreuz-1 has maintained 1904 cycles. Some applied load–macrostrain responses of the gage placed on the leg selected from all steps are shown in Fig. 23.

2.1.4. *Residual Macrostrain during the Step-by-Step Biaxial Cycling.* The six steps were performed during the biaxial LCF testing of Kreuz-1. After each step the strain gages fixed the residual macrostrains (Fig. 24). Unfortunately, the gages placed on the membrane have not stood plenty of cycles. The A1_leg strain gage has fixed the compression residual macrostrain of about -0.03% at the end of the cycling.

2.2. Sample Kreuz-2. The five FCA-5-11 strain gages were placed on Kreuz-2 (Table 2 and Fig. 25). The cycling of the sample was made step by step at the frequency of 0.5 Hz.

2.2.1. *In-Plane Biaxial LCF Tension–Compression Testing.*

- 1st step: the load of 15 kN, the step cycle number of 500.

Indicated values of the load control devices and the strain gages during the 1st step are shown in Figs. 26–30. The applied load–macrostrain responses of the gages placed on the membrane are shown in Fig. 31.

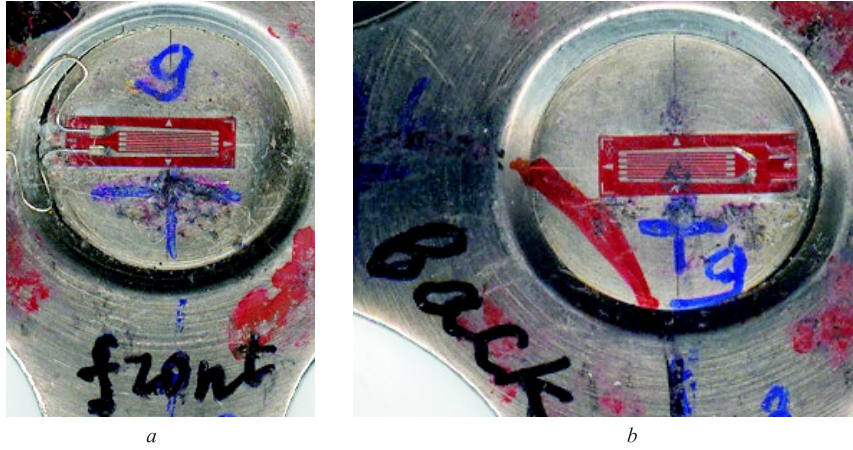


Fig. 22. Membrane crack of Kreuz-1: *a* — the front side; *b* — the back side of the membrane

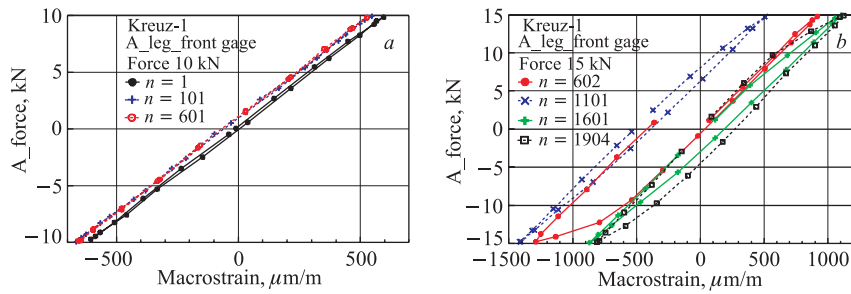


Fig. 23. Applied load–macrostrain responses of the strain gage on the front side of the A1_leg selected from all steps: *a* — the load of 10 kN; *b* — the load of 15 kN

- 2nd step: the load of 15 kN, the step cycle number of 500, the full cycle number of 1000.

Indicated values of the strain gages during the 2nd step are shown in Figs. 32–34. The strain gages on the membrane did not maintain tests and consistently failed: the A_front gage on the 275th cycle, the B_back gage on the 345th cycle, the A_back gage on the 365th cycle. Only the B_front strain gage has remained whole up to the end of the 2nd step. The applied load–macrostrain responses of the gages placed on the membrane are shown in Fig. 35.

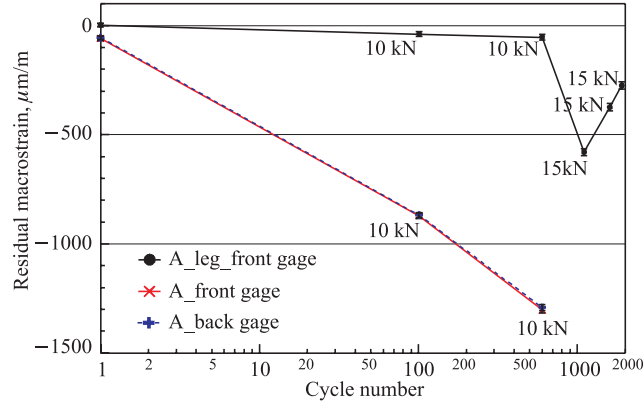


Fig. 24. Residual macrostrain in Kreuz-1

Table 2. Strain gages on Kreuz-2

Sample side	Front		Back	
Load direction	A1-A2	B1-B2	A1-A2	B1-B2
Gage name	A_front ($r = 0$)	B_front ($r = 0$) B_leg_front ($r = 18.5$ mm)	A_back ($r = 0$)	B_back ($r = 0$)

- 3rd step: the load of 15 kN, the step cycle number of 200, the full cycle number of 1200.

Indicated values of the strain gages during the 3rd step are shown in Figs. 36–37. The last B_front strain gage on the membrane did not maintain the tests and failed on the 118th cycle. The applied load–macrostrain responses of the B_front strain gage are shown in Fig. 38.

After the 3rd step three steps on 100, 100 and 200 cycles, respectively, were performed. The 6th step was the last one. Thus, Kreuz-2 was subjected to the full cycle number of 1600 that was more than Kreuz-1, but the membrane of Kreuz-2 has remained unbroken. Further cycling of the sample was stopped.

2.2.2. *Residual Macrostrain during the Step-by-Step Biaxial Cycling.* The six steps were performed during the biaxial LCF testing of Kreuz-2. After each step the strain gages fixed the residual macrostrains (Fig. 39). Though the strain gages on the membrane have appeared more crash-proof, nevertheless, they have not maintained up to the end of the testing. The B1_leg strain gage fixed the tension residual macrostrain of about -0.008% at the end of the cycling.

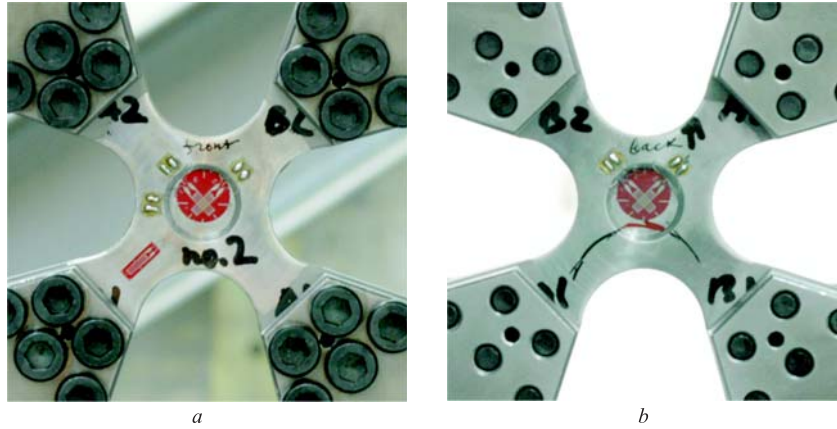


Fig. 25. Placing of the strain gages on Kreuz-2: *a* — front side; *b* — back side

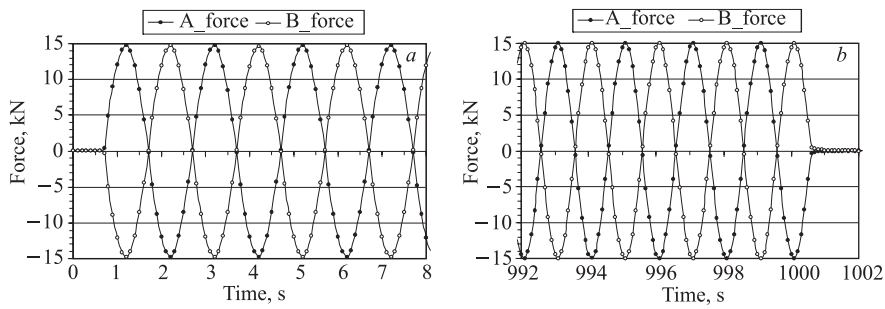


Fig. 26. Biaxial tension–compression loads applied to Kreuz-2: *a* — beginning of the 1st step; *b* — ending of the 1st step

2.3. Sample Krest-1. In this case, the testing of Krest-1 was not controlled by the strain gages (Fig. 40). During this testing the same cycling parameters as for Kreuz-2 were used, i. e., the load amplitude of 15 kN, the frequency of 0.5 Hz. The cycling of the sample was made step by step.

2.3.1. In-Plane Biaxial LCF Tension–Compression Testing. The four steps on 500 cycles each were performed during the testing of Krest-1. Further cycling of the sample was stopped. Thus, Krest-1 was subjected to the full cycle number of 2000 that was more than that of Kreuz-2, but the membrane of Krest-1 has remained unbroken.

2.4. Sample Krest-2. At the testing of Krest-2 an attempt to a higher cycling frequency was made but it appeared unsuccessful. The testing of Krest-2 was

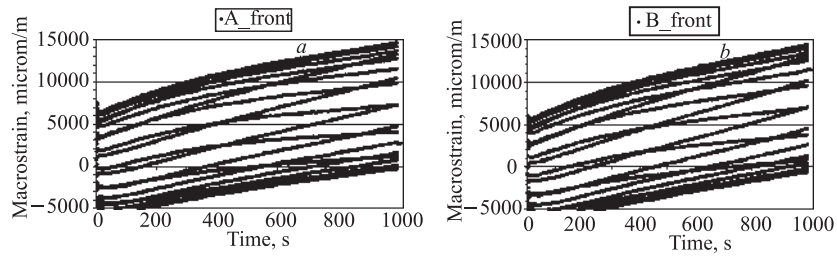


Fig. 27. Signals of the strain gages on the front side of the membrane (1st step): *a* — A1–A2 direction; *b* — B1–B2 direction

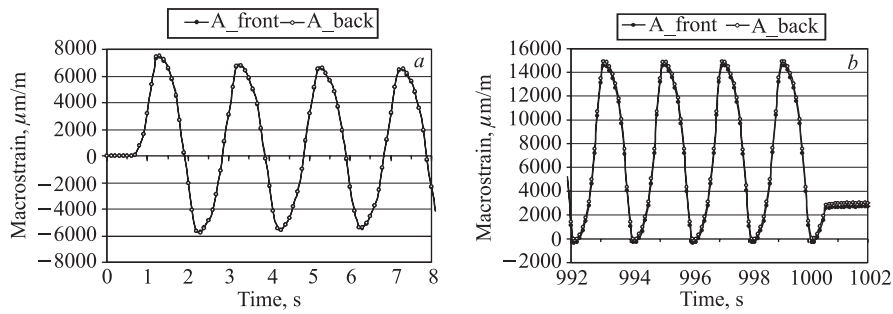


Fig. 28. Signals of the A1–A2 direction strain gages on the front and back sides of the membrane: *a* — beginning of the 1st step; *b* — ending of the 1st step

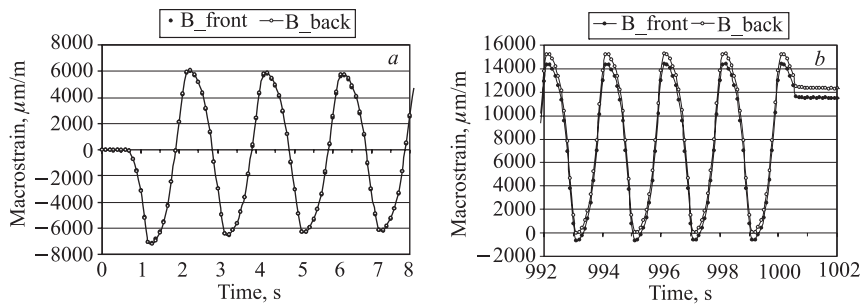


Fig. 29. Signals of the B1–B2 direction strain gages on the front and back sides of the membrane: *a* — beginning of the 1st step; *b* — ending of the 1st step

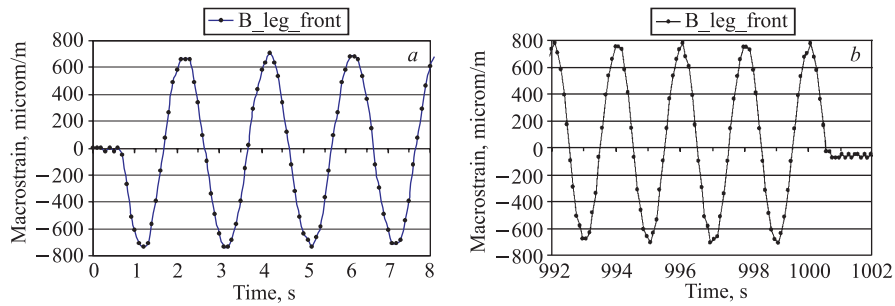


Fig. 30. Signal of the strain gage on the front side of the B1_leg: *a* — beginning of the 1st step; *b* — ending of the 1st step

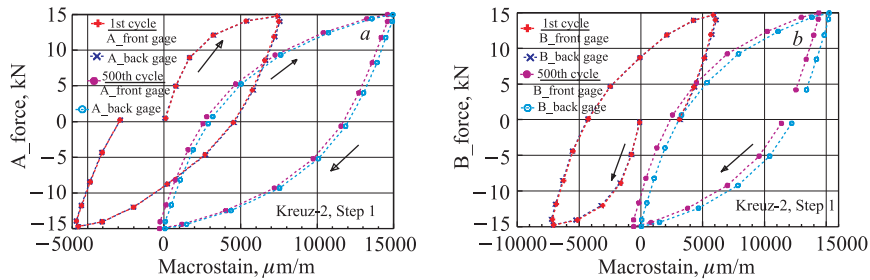


Fig. 31. Applied load–macrostrain responses of the strain gages on the membrane of Kreuz-2 (1st step): *a* — A1–A2 direction; *b* — B1–B2 direction

continued at the same frequency as that of Krest-1 but with the greater load. The cycling of the sample was made step by step.

2.4.1. In-Plane Biaxial LCF Tension–Compression Testing.

- 1st step: the load of 17 kN, the frequency of 5 Hz, the step cycle number of 22.

During this step an attempt to make the HCF testing was undertaken. But the instability of the testing machine was displayed at the high frequency of 5 Hz. After the 22nd cycle the testing was stopped.

- 2nd step: the load of 17 kN, the frequency of 0.5 Hz, the step cycle number of 57.

To check the machine operation the frequency was decreased down to 0.5 Hz. Any problems were not displayed at low frequency, the machine worked properly.

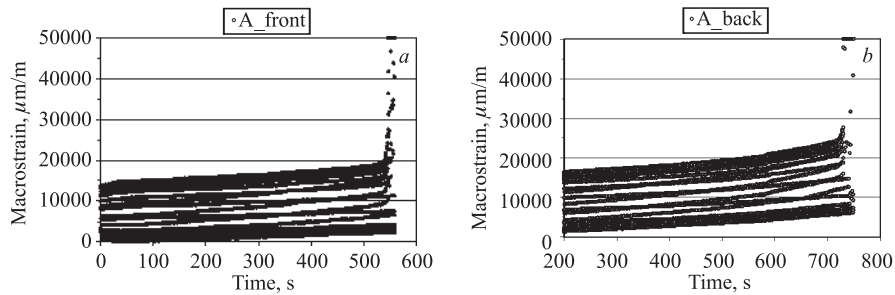


Fig. 32. Signals of the A1–A2 direction strain gages on the membrane (2nd step): *a* — front side; *b* — back side

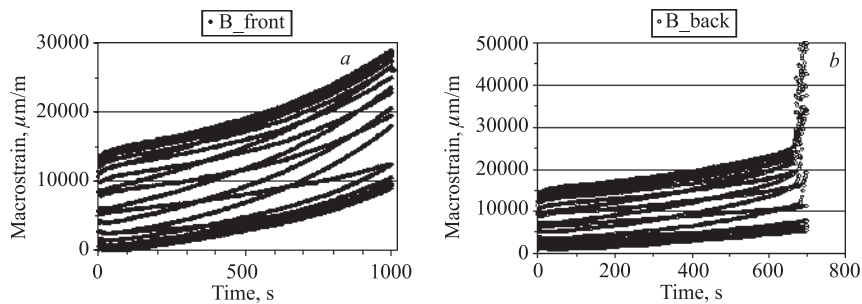


Fig. 33. Signals of the B1–B2 direction strain gages on the membrane (2nd step): *a* — front side; *b* — back side

- 3rd step: the load of 17 kN, the frequency of 2 Hz, the step cycle number of 71.

Next attempt to make the HCF testing was undertaken at the frequency of 2 Hz. However, the machine did not work properly. After the 71st cycle the testing was stopped.

- 4th step: the load of 17 kN, the frequency of 0.5 Hz, the step cycle number of 50, the full cycle number of 107 at the frequency of 0.5 Hz.

After the 4th step six steps on 500 cycles each were performed at the low frequency of 0.5 Hz. Further cycling of the sample was stopped. Thus, Krest-2 was subjected to the full cycle number of 407 at the frequency of 0.5 Hz not including the cycling at the higher frequencies, but the membrane of the sample has remained unbroken.

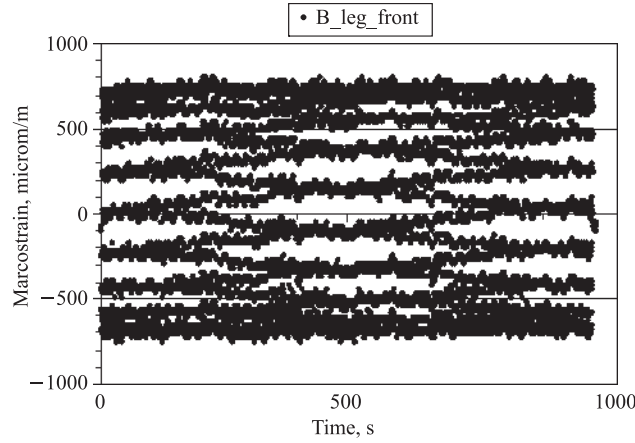


Fig. 34. Signal of the strain gage on the front side of the B1_leg (2nd step)

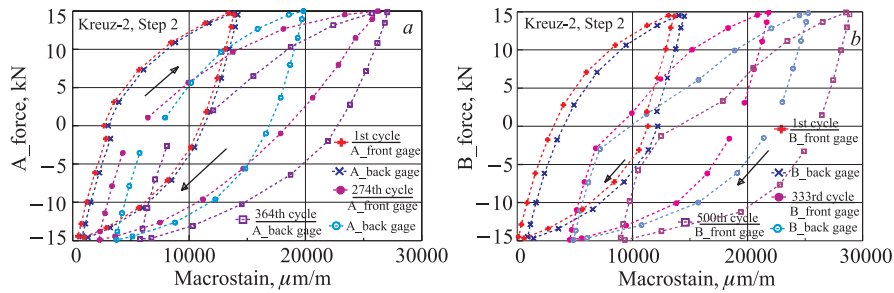


Fig. 35. Applied load-macrostrain responses of the strain gages on the membrane of Kreuz-2 (2nd step): *a* — A1-A2 direction; *b* — B1-B2 direction

CONCLUSION

The in-plane biaxial low cycle fatigue of austenitic stainless steel was performed on the Instron 100 kN biaxial planar cruciform system at FIMS. The samples of the cruciform geometry were made from a low carbon Ti-alloyed metastable austenitic stainless steel of the Russian grade GOST 12X18H10T (which is an analogue of the US grade AISI 321 H).

Two different designs of the samples of the cruciform geometry were carried out at FIMS and FLNP. The two pairs of the samples were machined in the FLNP workshop under the FIMS and FLNP designs, respectively.

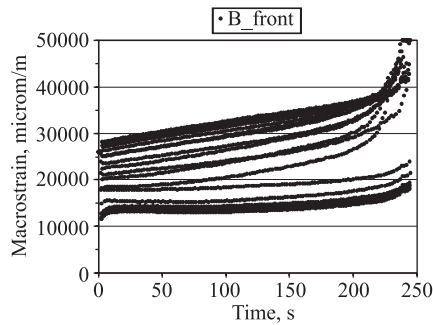


Fig. 36. Signal of the B1-B2 direction strain gage on the membrane front side (3rd step)

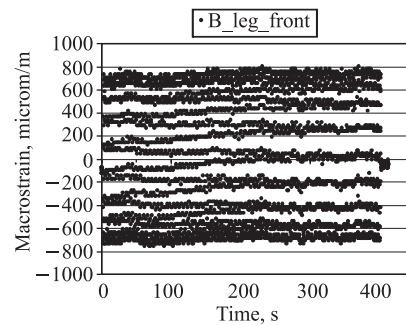


Fig. 37. Signal of the strain gage on the front side of the B1_leg (3rd step)

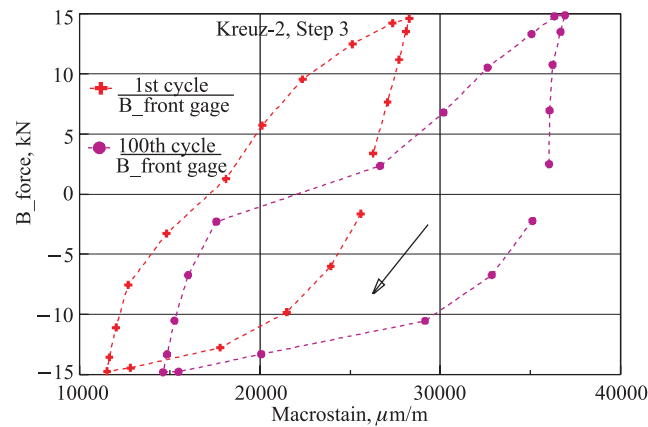


Fig. 38. Applied load-macrostrain responses of the B-front strain gage of Kreuz-2 (3rd step)

One sample from each pair was planned during the testing to finish by break to define the maximum number of cycles that a sample is capable to stand. The second sample from each pair would be cycled up to 85–90% of the maximum number of cycles.

This intention was maintained for the samples of the FIMS design (the samples of Kreuz-1 and Kreuz-2). Kreuz-1 was broken during the 1904th cycle at the load of 15 kN. Kreuz-2 was cycled at the load of 15 kN up to 1600 cycles and it has remained unbroken as it was expected.

Another situation has developed during the testing of the samples of the FLNP design (the samples of Krest-1 and Krest-2). Krest-1 was cycled up to 2000 cycles

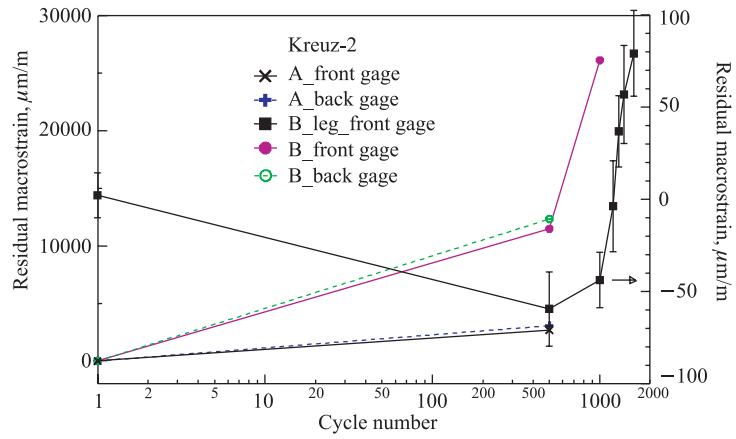


Fig. 39. Residual macrostrain in Kreuz-2

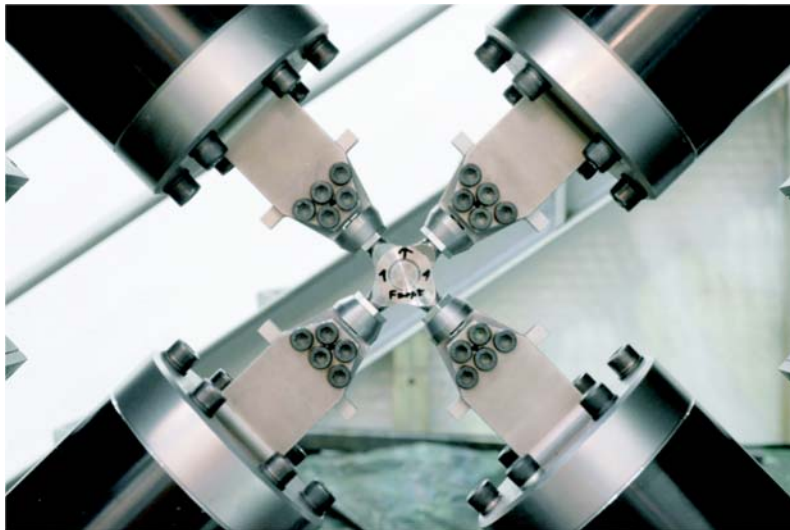


Fig. 40. Front side of Krest-1

at the load of 15 kN and it has remained unbroken that was not expected. The further test was stopped as the primitive estimation using a permanent magnet probe has shown that the content of the martensite phase in Krest-1 was not less than that in the broken Kreuz-1. Krest-2 was cycled at the load increased to 17 kN instead of 15 kN up to 407 cycles and it has also remained unbroken.

Only samples of Kreuz-1 and Kreuz-2 were equipped with strain gages to obtain information from the sample membrane and one of four legs that connected the sample with the testing machine. Unfortunately, the strain gages on the membrane have not stood the testing up to the end and, thus, there are only partial information about plastic flow and residual macrostrain. The strain gages on the legs worked properly up to the end.

Nevertheless, some interesting phenomena were observed during the cycling of Kreuz-1 and Kreuz-2:

1. The response cycle loops of the strain gages on the membrane of the sample of Kreuz-1 were symmetrical and practically closed during the cycling with the load of 10 kN (Figs. 9, 13 and 15).
2. At increase of the load up to 15 kN for the same sample at the beginning of the cycling the loop has appeared strongly nonclosed, however, with increase of number of cycles the loop openness was smoothed out (Fig. 19).
3. The same picture as described for Kreuz-1 was observed for Kreuz-2, which was at once cycled with the load of 15 kN (Fig. 31). Furthermore, with further increase of number of cycles the loop was rather strongly deformed (Figs. 35 and 38).
4. The residual macrostrain on the membrane of Kreuz-1 along the A1–A2 direction was already negative (compression) after the 1st cycle (Fig. 24). The residual compression is increased with accumulation of cycles.
5. The opposite picture was observed for the sample of Kreuz-2 (Fig. 39). The residual macrostrains on the membrane along both directions were positive (tension) after the 1st cycling step. The residual tension is increased with accumulation of cycles (the B1–B2 direction). In this case, the rate of growth of the residual tension was higher in the B1–B2 direction than in the A1–A2 direction.
6. Regarding the residual macrostrain on the front leg of Kreuz-1, residual compression was observed in the A1–A2 direction (Fig. 24). The compression is increased with accumulation of cycles.
7. The residual macrostrain on the front leg of Kreuz-2 in the B1–B2 direction has become negative (compression) after the 1st cycling step (Fig. 39). However, the residual macrostrain began to increase with accumulation of cycles and has changed its sign (from compression to tension) during the last cycling steps.

The *ex-situ* fatigued samples of Kreuz-1 and Kreuz-2 were sent to FINT to perform some optical microscopy and Barkhausen magnetic noises investigations.

The results of these measurements will be published later. The *ex-situ* fatigued samples of Krest-1 and Krest-2 were brought in FLNP and in October 2007 were preliminary tested by neutron diffraction method at the IBR-2 pulsed nuclear reactor (FLNP JINR) with the goal of determination of martensite volume fraction and estimation of the beam time for full experiments. The results were the following: Krest-1 and Krest-2 have exhibited the martensite volume fraction of 17.4 and 38.7%, respectively. In November–December 2006, the neutron diffraction stress analysis of the Krest-1 sample was performed at the IBR-2 reactor, the results of which contains the content of the 2nd part of the present paper.

REFERENCES

1. Lohr R. // ASTM STP. 2001. V. 1387. P. 355–367.
2. Daymond M.R., Schreiber J., Taran Yu.V. // J. Neutron Research. 2001. V. 9, Nos. 2–4. P. 207–215.
3. Taran Yu.V., Daymond M.R., Eifler D. et al. // Materials Science Forum. 2002. V. 404–407. P. 501–508.
4. Taran Yu.V., Daymond M.R., Schreiber J. // J. Neutron Research. 2003. V. 11, No. 4. P. 255–261.
5. Taran Yu.V., Daymond M.R., Schreiber J. // Physica B. 2004. V. 350, Issues 1–3. P. 98–101.
6. Taran Yu.V. et al. // Materials Science and Technology. 2005. V. 21, No. 1. P. 35–45.
7. Taran Yu.V. et al. // Proc. of Stainless Steel World 2005 Conference, Maastricht, the Netherlands, 8–10 November 2005, KCI Publishing BV, P. 357–362.
8. Taran Yu.V., Daymond M.R., Schreiber J. // Zeitschrift für Kristallographie. 2006. Supplement Issue No. 23. S. 345–350.
9. Taran Yu.V. et al. // Materials Science Forum. 2006. V. 524–525. P. 899–904.

Received on July 18, 2007.

Редактор *В. В. Булатова*

Подписано в печать 10.01.2008.

Формат 60 × 90/16. Бумага офсетная. Печать офсетная.

Усл. печ. л. 1,75. Уч.-изд. л. 2,49. Тираж 290 экз. Заказ № 56017.

Издательский отдел Объединенного института ядерных исследований
141980, г. Дубна, Московская обл., ул. Жолио-Кюри, 6.

E-mail: publish@jinr.ru

www.jinr.ru/publish/